Ultrafast Relaxation of Zinc Protoporphyrin Encapsulated within Apomyoglobin in Buffer Solutions

Liyang Luo,[†] Chin-Hao Chang,[‡] Yue-Ching Chen,[†] Tung-Kung Wu,*[,‡] and Eric Wei-Guang Diau*[,†]

Department of Applied Chemistry and Institute of Molecular Science and Department of Biological Science and Technology, National Chiao Tung University, Hsinchu 30010, Taiwan

Received: December 8, 2006; In Final Form: April 28, 2007

The relaxation dynamics of a zinc protoporphyrin (ZnPP) in THF, KPi buffer, and encapsulated within apomyoglobin (apoMb) was investigated in its excited state using femtosecond fluorescence up-conversion spectroscopy with S_2 excitation ($\lambda_{ex} = 430$ nm). The $S_2 \rightarrow S_1$ internal conversion of ZnPP is ultrafast ($\tau < 100$ fs), and the hot S_1 ZnPP species are produced promptly after excitation. The relaxation dynamics of ZnPP in THF solution showed a dominant offset component ($\tau = 2.0$ ns), but it disappeared completely when ZnPP formed aggregates in KPi buffer solution. When ZnPP was reconstituted into the heme pocket of apoMb to form a complex in KPi buffer solution, the fluorescence transients exhibited a biphasic decay feature with the signal approaching an asymptotic offset: at $\lambda_{em} = 600$ nm, the rapid component decayed in 710 fs and the slow one in 27 ps; at $\lambda_{em} = 680$ nm, the two time constants were 950 fs and 40 ps. We conclude that (1) the fast-decay component pertains to an efficient transfer of energy from the hot S_1 ZnPP species to apoMb through a dative bond between zinc and proximal histidine of the protein; (2) the slow-decay component arises from the water-induced vibrational relaxation of the hot S_1 ZnPP species; and (3) the offset component is due to $S_1 \rightarrow T_1$ intersystem crossing of the surviving cold S_1 ZnPP species. The transfer of energy through bonds might lead the dative bond to break, which explains our observation of the degradation of ZnPP-Mb samples in UV−vis and CD spectra upon protracted excitation.

Introduction

As an excellent system to harvest light, metallo-porphyrins play significant roles both as biological reaction centers[1−3] and in optoelectronic applications such as dye-sensitized solar cells.[4,5] Among many investigations of the spectra and dynamics of porphyrins, the photophysical properties of zinc porphyrins in solution[6−9] and functionalized on a TiO_2 thin-film surface[10−13] have been extensively investigated, providing much information on the mechanism of relaxation of excited porphyrins in various environments.

Zinc protoporphyrin IX (ZnPP), a metabolic intermediate with iron replaced by zinc in the substituted porphyrin center, is involved in the absolute iron deficiency in hemeodialysis patients and has been integrated into an artificial photosynthetic system.[14] ZnPP forms a monolayer on a gold surface through a carboxyl functional group, which provides a way to immobilize natural porphyrins on solid substrates.[15] Similarly, ZnPP molecules were successfully immobilized on the surface of nanochannel arrays of anodized aluminum oxide (AAO); excitonic coupling due to aggregation of ZnPP inside the nanoporous environment produces a broadening of the absorption spectrum to cover the entire visible region.[16] Because of the efficient intermolecular transfer of energy through $\pi-\pi$ stacking interactions, the aggregation behavior in porphyrins has attracted much attention.[4,13,16−22] Despite ZnPP having two propanoic acid side chains attached to the aromatic ring, it does not dissolve readily in aqueous solution. Protoporphyrin IX, a free base form of ZnPP, is reported to form aggregates in aqueous solution; the extent of aggregation is controllable through the pH of the solution.[22]

Protein dynamics are well-recognized to be an important issue in understanding the relationships between structure and function in biological systems.[23−26] Being a model system, myoglobin (Mb) is an intensively studied protein. An understanding of the biological function of Mb requires dynamical information about the interactions between the heme group and its pocket. The dynamics of electronic and thermal relaxation of Mb in aqueous solution have accordingly been investigated using time-resolved fluorescence,[27] IR,[28] femtosecond pump−probe,[29] and resonance Raman spectral[25] methods as well as with simulations of molecular dynamics.[23,30] Because the lifetime of a heme molecule in its excited state is as small as ~1 ps,[28] the relaxation in heme proteins occurs mostly in the electronic ground state. In an investigation of the relaxation kinetics with the most sensitive method, −fluorescence decay, artificially fluorescent protein was made on removing the heme molecule from Mb to form an apomyoglobin (apoMb) and reconstituting the ZnPP molecule into the heme pocket of the protein.[31−35] Under such conditions, the kinetics of electron transfer induced by light has been investigated from the triplet states of ZnPP-Mb and other Mb-based triad systems.[31−36]

In the present work, we show that ZnPP molecules form aggregates in KPi buffer solution but that the ZnPP monomer can be isolated either in an organic solvent (THF) or embedded inside the active site of apoMb in a buffer solution. Measurements of UV−vis spectra, time-resolved fluorescence anisotropies, and circular dichroism (CD) assays provide evidence for

* Corresponding author. Fax: (886)-03-572-3764; e-mail: tkwmll@mail.nctu.edu.tw; diau@mail.nctu.edu.tw.
[†] Department of Applied Chemistry and Institute of Molecular Science.
[‡] Department of Biological Science and Technology.

10.1021/jp068449n CCC: $37.00
Published on Web 06/13/2007

the formation of a stable ZnPP-Mb complex in aqueous solution. On the basis of both picosecond time-correlated single-photon counting (TCSPC) and femtosecond fluorescence up-conversion methods, explicit experimental evidence is provided for the manner in which a protein matrix influences the relaxation of ZnPP through a comparison of the fluorescence dynamics of ZnPP in THF, KPi buffer (100 mM), and reconstituted within apoMb. A time scale, sub-picoseconds, is given for energy to transfer from ZnPP to apoMb through the dative bond between the zinc atom and the proximal histidine of the protein. By means of UV−vis and CD spectra, we observed also the degradation of ZnPP-Mb samples upon protracted excitation, implying that the efficient transfer of energy through bonds might eventually lead to dissociation.

Experimental Procedures

Preparation of apoMb. Apomyoglobin was prepared by the modified butanone method to extract heme.[37] In summary, Mb (0.1 g) was dissolved in ice-cold, salt-free PBS (30 mL) before the pH was set to 2.0. The heme prosthetic group was extracted on adding HCl (0.1 M) dropwise to the solution. The acid denatured Mb solution was mixed with an equal volume of ice-cold butanone and shaken until formation of a hazy pale-yellow protein layer and a dark-brown heme-containing layer. The aqueous layer was repeatedly extracted with ice-cold butanone to remove residual heme from Mb. After this heme extraction, the apoMb solution was dialyzed against doubly distilled H_2O twice, then dialyzed extensively against potassium phosphate (10 mM, pH 7.0) overnight. The apoMb was then lyophilized and preserved at −20 °C until use.

Reconstitution of apoMb with ZnPP. To reconstitute zinc (II) protoporphyrin into apomyoglobin, we followed the modified method of Hamachi et al.[36,38] ZnPP (1.5 molar proportion) in a KPi/pyrimidine (100 mM, 1:1, v/v) solution (5.2 mM, 1.66 mg) was added dropwise to an apomyoglobin solution (0.235 mM) in 100 mM KPi/DMSO (4:1) buffer pH 12 (7.5 mL) cooled in an ice bath. After incubation for 15 min, the solution was adjusted to pH 6.8 and slowly stirred at 4 °C for an additional 6 h. The solution was transferred into a dialysis membrane against doubly distilled H_2O, with two changes of H_2O to remove organic solvent, followed by additional dialysis against KPi buffer (100 mM, pH 6.8) overnight. The solution was then filtered with a cellulose membrane (0.2 μm) before being applied to a column (Sephadex G-25), equilibrated with KPi buffer (100 mM, pH 6.8), and eluted with the same buffer at 4 °C. The protein band was collected and stored at −20 °C for subsequent experiments.

Steady-State Spectral Measurements. We recorded UV−vis absorption spectra of ZnPP in THF, in KPi buffer, and encapsulated in apoMb with a standard spectrophotometer (Cary 50, Varian) and emission spectra with a composite CCD spectrometer (USB2000FLG, Ocean Optics); the excitation source of the latter contains a pulsed diode-laser head (LDH-P-C-400, PicoQuant) coupled with a laser-diode driver (PDL-800B, PicoQuant) that produces excitation pulses at 405 nm with an average power of ∼300 μW. We recorded CD spectra with a spectropolarimeter (J-715, JASCO) and a thermostated quartz cuvette (path length 1 mm) at 23 °C.

Time-Resolved Fluorescence Measurements. To measure lifetimes on a picosecond scale and anisotropy, we used a time-correlated single-photon counting spectrometer (TCSPC, FluoTime 200, PicoQuant), with excitation from either a femtosecond laser system (Verdi-V10 and Mira 900D, Coherent) at 430 nm (doubled from a 860 nm beam output) or a picosecond laser system (LDH-P-C-440 and PDL-800B, PicoQuant) at 435 nm; the instrument response is ∼30 ps with the femtosecond laser system but increases to ∼80 ps with the picosecond laser system.

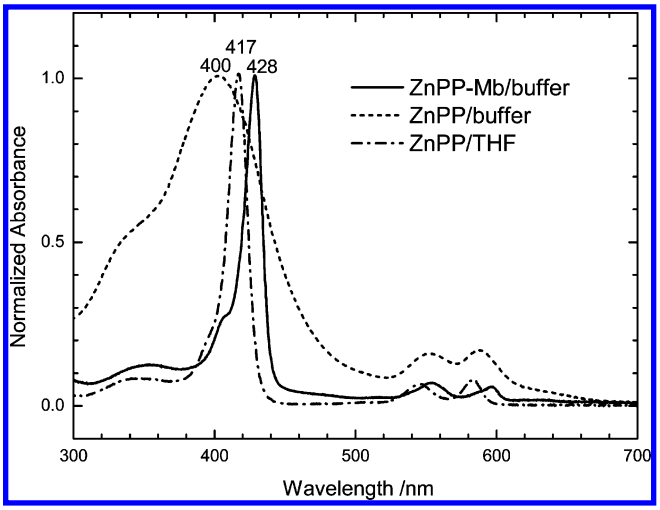

Figure 1. Normalized steady-state absorption spectra of ZnPP in THF (dashed−dotted curve), KPi buffer (dashed curve), and reconstituted inside the heme pocket of apomyoglobin (solid curve). The concentration of all samples was 5×10^{-6} M.

The experiment to measure the femtosecond up-conversion is described elsewhere.[13a] Briefly, the femtosecond laser system generates output pulses at 860 nm with a duration ∼150 fs at a repetition rate of 76 MHz. The frequency of the laser at 860 nm was doubled for excitation (λ_{ex} = 430 nm). The emission was collected with two parabolic mirrors and focused onto a crystal (BBO type I); the gate pulse was also focused onto the BBO crystal for sum-frequency generation. On varying the temporal delay between gate and excitation pulses via a stepping-mirror translational stage, we obtained a temporal profile. The polarization between pump and probe pulses was fixed at the magic angle 54.7°.

Results and Discussion

Steady-State Spectra of ZnPP in Various Environments. We compare the steady-state spectra of ZnPP in THF, in KPi buffer (100 mM), and reconstituted into the apoMb heme pocket to form a ZnPP-Mb complex in buffer solution. Figure 1 displays absorption spectra of ZnPP in the range of 300−700 nm in these conditions: ZnPP in THF is shown as a dashed−dotted curve; ZnPP in KPi buffer solution (100 mM, pH 6.8) is shown as a dashed curve; and ZnPP encapsulated within apoMb in KPi buffer solution is shown as a solid curve. The absorption spectra all exhibit two prominent features, the Soret (or B) band and the Q bands, traditionally identified as the $S_2 \leftarrow S_0$ and $S_1 \leftarrow S_0$ transitions, respectively. Explicitly, the maxima of these bands in ZnPP/THF solution at 417, 545, and 583 nm are assigned as B(0,0), Q(1,0), and Q(0,0), respectively; the number of quanta shown in parentheses represents the dominant Franck−Condon active vibrational modes.[8,13a]

The Soret band of ZnPP in KPi buffer became much broader than that of ZnPP in THF, whereas no appreciable change was observed for the Q bands.[39] A red-shift was observed for both the Soret and the Q bands of ZnPP-Mb in KPi buffer solution. Because the energy of a typical $\pi-\pi^*$ state in porphyrins decreases with increasing solvent polarity,[40] the energy gap of the $S_0 \rightarrow S_1$ transition of ZnPP or ZnPP-Mb in a buffer is smaller than that of ZnPP in THF, which is consistent with the red-shifted spectral feature of the Q band of the former with respect to the latter. The same is true for the $S_0 \rightarrow S_2$ transition of ZnPP-

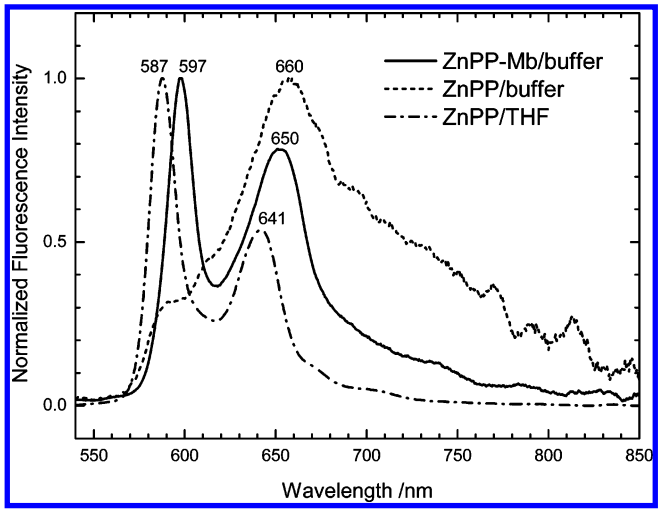

Figure 2. Normalized steady-state fluorescence spectra of ZnPP in THF (dashed−dotted curve), KPi buffer (dashed curve), and encapsulated within apomyoglobin (solid curve) with excitation at the Soret band. The sample concentration was 5×10^{-6} M.

Mb in KPi buffer for which a red-shift of 11 nm was observed for the Soret band relative to ZnPP in THF. In contrast, the Soret band of ZnPP in KPi buffer was blue-shifted by 17 nm. The broad and blue-shifted spectral features of ZnPP in KPi buffer are generally attributed to the formation of ZnPP aggregates of H type in aqueous solution.[17,22,41,42] When ZnPP was encapsulated within the active site of an apomyoglobin to form a ZnPP-Mb complex in buffer solution, the Soret band of the complex became sharp and shifted toward larger wavelengths, as we have observed.

The emission spectra of ZnPP in various environments are shown in Figure 2. The fluorescence spectrum of ZnPP in THF exhibits a typical mirror image of the Q band of the corresponding absorption spectrum shown in Figure 1. Accordingly, the fluorescence maxima are assigned as Q(0,0) at 587 nm and Q(0,1) at 641 nm. Similarly, the fluorescence spectrum of ZnPP-Mb in buffer solution also shows a mirror image of the Q band but with the two emission maxima red-shifted by ∼10 nm with respect to those of ZnPP in THF. This spectral feature provides strong evidence for the ZnPP monomer being bound firmly into the heme pocket of the apoMb in the ZnPP-Mb/buffer solution—the bathochromic shift in the emission spectrum is consistent with the spectral shift in the absorption spectrum of the system. In contrast, when the ZnPP molecules aggregate in the absence of the protein matrix in a buffer solution, the typical emission feature of a ZnPP monomer disappears. The fluorescence maximum of ZnPP in a buffer solution became significantly red-shifted to 660 nm, and the intensity corresponding to the ZnPP monomer ($\lambda_{em} = \sim 590$ nm) became much smaller than that in ZnPP/THF or the ZnPP-Mb/buffer solution. Because the fluorescence was significantly quenched in the ZnPP/buffer solution, intermolecular transfer of energy is expected to be efficient when the ZnPP molecules aggregate (Figure 1). We thus attribute the quenching of the fluorescence to the aggregation of ZnPP in the KPi buffer; incorporation of the ZnPP into the heme pocket of apoMb inhibits the intermolecular transfer of energy and thus prevents the quenching of ZnPP fluorescence.

Stability of the ZnPP-Mb Complex. To test the photostability of the ZnPP-Mb complex, we measured the absorption spectra of the ZnPP-Mb/buffer samples under femtosecond laser irradiation at 430 nm (power = ∼5 mW) for several durations of excitation. The reconstituted proteins became denatured to some extent when the samples were exposed to this radiation. Figure 3 shows absorption spectra of the ZnPP-Mb samples in a rotating cell (∼1 mm) with excitation periods 0, 10, 30, and 50 min at 23 °C. The absorbance at the maxima of both B and Q bands decreased with increasing duration of excitation (indicated by downward arrows), and the width of these absorption bands increased. In contrast, the broad absorptions at about 390, 470, and 620 nm increased with increasing excitation duration (indicated by upward arrows), leading to several isosbestic points being observed. The variation of the absorption spectra and the existence of these isosbestic points upon excitation reflect the photoinstability of the system, according to the following explanation. The ZnPP-Mb complexes first absorbed the excitation photons and relaxed to their lower electronic states via nonradiative transitions; this process transfers the excitation energy into the internal energy of the protein. Second, the internal energy of the system might be further transferred into the environment by solvent-induced vibrational relaxation that increases the thermal energy (or temperature) of the local environment. Third, dissociation of the ZnPP-Mb complex might occur in two steps: (1) if dissociation was more rapid than the energy transfer or (2) if dissipation of the thermal energy was too slow. In either step, the ZnPP-Mb complex decomposed so that ZnPP moved out of the heme pocket of the protein to form aggregates with other free ZnPP species. Because dissociation of ZnPP from the protein occurred upon excitation, we deduce that the binding of the zinc cation of ZnPP to the histidine group of apoMb is weaker than that of heme in myoglobin.

We measured also the variation of the CD spectra to test the photostability of the reconstituted ZnPP-Mb complex. According to the reported CD spectrum of a protein, the characteristic α-helical conformation of myoglobin occurs in the spectral region of 200−250 nm.[43] In Figure 4, two negative ellipticity bands at 211 and 221 nm correspond to the conformational feature of the ZnPP-Mb complex. There is also a positive ellipticity band at about 428 nm corresponding to the characteristic absorption spectral feature of ZnPP. No signal was observed in the CD spectrum of the ZnPP/buffer solution (Figure 4, trace f). When the periods of laser excitation increased from 0 to 60 min, the strength of the two negative ellipticity bands and the one positive ellipticity band systematically decreased (Figure 4, traces a−e). Fandrich et al.[44] proved that the α-helical conformation of Mb was progressively lost when the temperature was increased above 40 °C. In our case, the unfolding state of the reconstituted ZnPP-Mb complex was attained to induce progressive loss of the α-helical conformation either through excess internal energy absorbed by ZnPP or through the thermal energy of the local environment. When the free ZnPP molecules aggregated in buffer solution, no band about 428 nm was observed in the CD spectrum. When the reconstituted ZnPP-Mb complex unfolded upon excitation, ZnPP would therefore be released to form aggregates in buffer solution, causing the decreased CD intensity at 428 nm as we have observed.

Picosecond Fluorescence Decays and Anisotropy Dynamics. For picosecond fluorescence measurements of ZnPP in various environments at 295 K, excitation was at $\lambda_{ex} = 435$ nm, and emission was observed in a broad wavelength range. Figure 5A−D shows four typical fluorescent decays of a ZnPP-Mb/buffer solution observed at λ_{em} (nm) = 590, 650, 710, and 770. The fluorescence transients are well-fitted with a biexponential decay function and two time constants τ_1 and τ_2; these fitted time constants and the corresponding relative amplitudes are summarized in Table 1. The values $\tau_1 = \sim 0.5$ ns and $\tau_2 =$

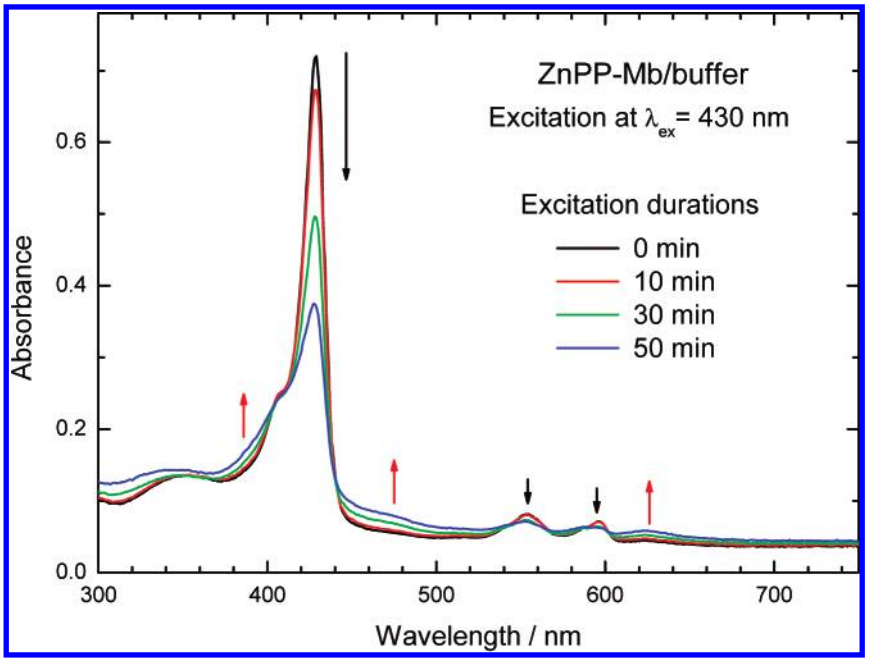

Figure 3. Steady-state absorption spectra of reconstituted ZnPP-Mb in buffer solution under femtosecond excitations with irradiation periods as indicated. The power of the excitation pulse is about 5 mW. The upward and downward arrows represent the systematic variation of absorbance as a function of duration of irradiation.

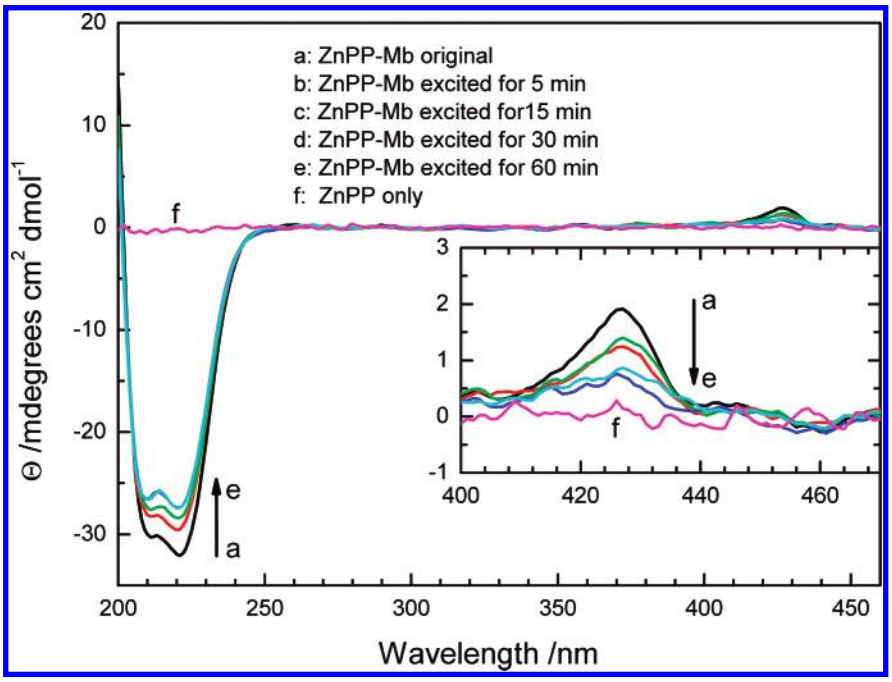

Figure 4. Circular dichroism (CD) spectra of reconstituted ZnPP-Mb in buffer solution under femtosecond excitations with irradiation periods as indicated. There are two negative ellipticity bands at 211 and 221 nm and one positive ellipticity band at 428 nm. The strength of the negative and positive ellipticity bands decreases when the duration of laser excitation increases.

2.2 ns are almost constant for $\lambda_{em} = 580-710$ nm, but both τ_1 and τ_2 decrease for $\lambda_{em} > 710$ nm. The relative amplitudes of the two components depend strongly on λ_{em} (i.e., the slow-decay component (τ_2) is the major part of the transient at smaller wavelengths, whereas the rapid-decay component (τ_1) becomes dominant at greater wavelengths). In view of the lifetime of a monomeric ZnPP in THF being $\tau = 2.07$ ns,[45] it is reasonable to assign the 2 ns component of the transient in ZnPP-Mb/buffer solution to the $S_1 \rightarrow T_1$ intersystem crossing (ISC) of the monomeric ZnPP inside the heme pocket of apoMb. According to the systematic variation of the relative amplitudes of the two components, the sub-nanosecond component that became significant at larger wavelengths reflects the contribution of free ZnPP molecules outside the apoMb active site in the form of ZnPP aggregates in buffer solution.

To provide evidence that the slow-decay component of the transients observed at shorter wavelengths was due to the contribution of the ZnPP-Mb complex, we measured the time-dependent fluorescence anisotropy of the system at $\lambda_{em} = 590$ nm. The fluorescence anisotropy at time t is expressed as[46]

$$r(t) = \frac{I_{VV} - GI_{VH}}{I_{VV} + G2I_{VH}} \quad (1)$$

in which $r(t)$ is the anisotropy at time t and I_{VV} and I_{VH} represent the time-dependent fluorescence intensities for excitation with

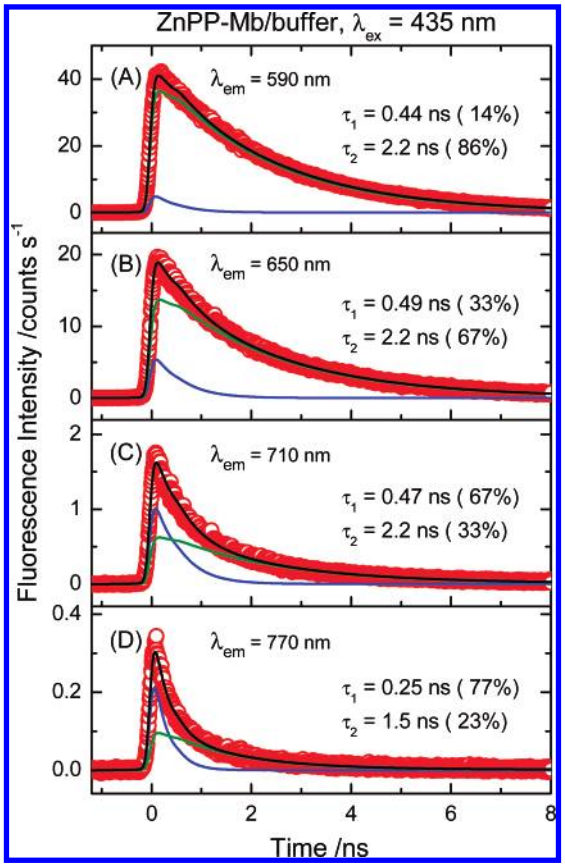

Figure 5. Picosecond fluorescence transients of reconstituted ZnPP-Mb in buffer solution with $\lambda_{ex} = 435$ nm at λ_{em} (nm) = (A) 590, (B) 650, (C) 710, and (D) 770. Two decay components served to describe the transients with a parallel kinetic model and the corresponding fitted time parameters as indicated; those of other wavelengths are listed in Table 1.

TABLE 1: Fitted Time Constants of Fluorescence Transients in ZnPP-Mb/Buffer Solutions with Excitation Wavelength $\lambda_{ex} = 435$ nm[a]

λ_{em} (nm)	τ_1 (ns)[b]	τ_2 (ns)[b]
580	0.44 (14%)	2.2 (86%)
590	0.44 (14%)	2.2 (86%)
610	0.53 (24%)	2.2 (76%)
630	0.52 (35%)	2.2 (65%)
650	0.49 (33%)	2.2 (67%)
670	0.51 (50%)	2.2 (50%)
690	0.50 (64%)	2.2 (36%)
710	0.47 (67%)	2.2 (33%)
730	0.44 (71%)	2.1 (29%)
750	0.32 (75%)	1.7 (25%)
770	0.25 (77%)	1.5 (23%)

[a] Parallel kinetic model is employed using the FluoFit software. [b] Relative amplitudes are shown in parentheses.

vertical polarization, but the polarizations of detection were made at the vertical (parallel) and horizontal (perpendicular) conditions for the former and the latter, respectively. Because the sensitivities through the monochromator with vertical and horizontal polarizations might not be equal, a correction was made with excitation at the horizontal polarization and the detection at either vertical (I_{HV}) or horizontal (I_{HH}) polarization (i.e., a factor $G = I_{HV}/I_{HH}$ was applied to correct the ratio I_{VV}/I_{VH}). According to the fluorescence decay data (refer to Supporting Information) analyzed with eq 1, we derived the anisotropy decays of both ZnPP/THF and ZnPP-Mb/buffer samples; the results are shown in Figure 6 for comparison.

The observed data for time-dependent anisotropy show three

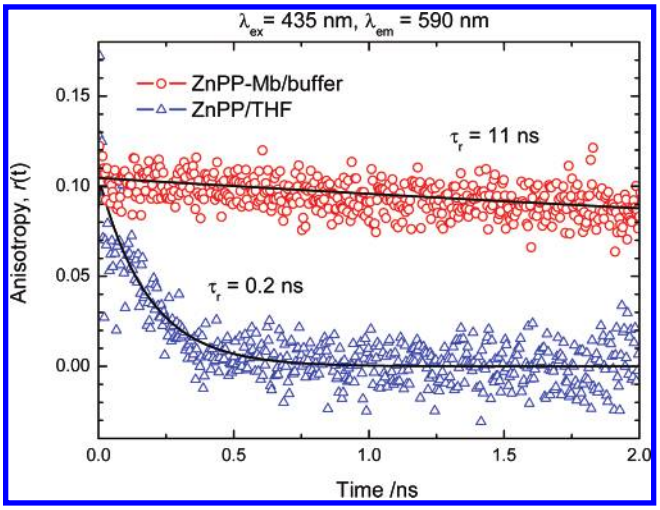

Figure 6. Picosecond fluorescence anisotropies of ZnPP in THF (triangles) and encapsulated within apomyoglobin in buffer solution (circles) obtained at $\lambda_{em} = 590$ nm with excitation at $\lambda_{ex} = 430$ nm.

important features. First, the values of $r(t)$ at zero delay time (r_0) in both systems are near 0.1, which is lower than the theoretical value (0.4) probably due to a different dipole orientation between the S_2 (excitation) and the S_1 (emission) states. Second, $r(t)$ gradually decays to zero for both samples (see Supporting Information), indicating that free rotation is involved in both systems. Third, a single-exponential decay function describes the decay feature of $r(t)$

$$r(t) = r_0 e^{-t/\tau_r} \quad (2)$$

in which the time constant τ_r represents the rotational correlation period of the system. We found the rotational correlation periods to be 0.2 ns for ZnPP/THF and 11 ns for ZnPP-Mb/buffer. The difference of τ_r between the two systems reflects the size of the system, as discussed next. When the ZnPP molecules are well-dispersed in THF solution, the free ZnPP molecules can freely reorientate; the reorientational period is the observed 0.2 ns. When the ZnPP monomers were encapsulated inside apoMb, such a reorientation of the ZnPP molecule inside the cavity of the protein was inhibited, however, and depolarization of ZnPP in its excited state might occur when the whole ZnPP-Mb complex made a movement in buffer solution. We observed that depolarization of the ZnPP-Mb system occurs on the time scale of 10 ns, which is 100 times that of the ZnPP/THF system.

Maiti et al. measured the time-resolved fluorescence anisotropy of ZnPP on S_1 excitation ($\lambda_{ex} = 580$ nm) in THF solution and in various micelles;[45] they reported the values $r_0 = 0.10$ and $\tau_r = 0.18$ ns in ZnPP/THF solution, which are identical to our results on S_2 excitation at $\lambda_{ex} = 435$ nm. When ZnPP was combined with micelles in aqueous solution, the time-dependent fluorescence anisotropy showed, however, a complicated dynamical feature that was described with two exponential decay functions. A wobble-in-cone model was considered to interpret such an observation (i.e., the fluorescence depolarization occurs on both rotational diffusion of ZnPP inside the micelle and the tumbling of the micelle).[45] In our case, only a single-exponential decay feature was observed for the fluorescence depolarization of ZnPP encapsulated inside apoMb, indicating that the ZnPP molecule was tightly bound to apoMb and reorientates with the entire protein molecule. Taking into account the effect of temperature with respect to the reorientational period, our observation for the ZnPP-Mb system, $\tau_r = 11$ ns, at 23 °C is consistent with the result of the TNS-Mb system, $\tau_r = 20.5$ ns, obtained at 2 °C with frequency-domain phase modulation.[47]

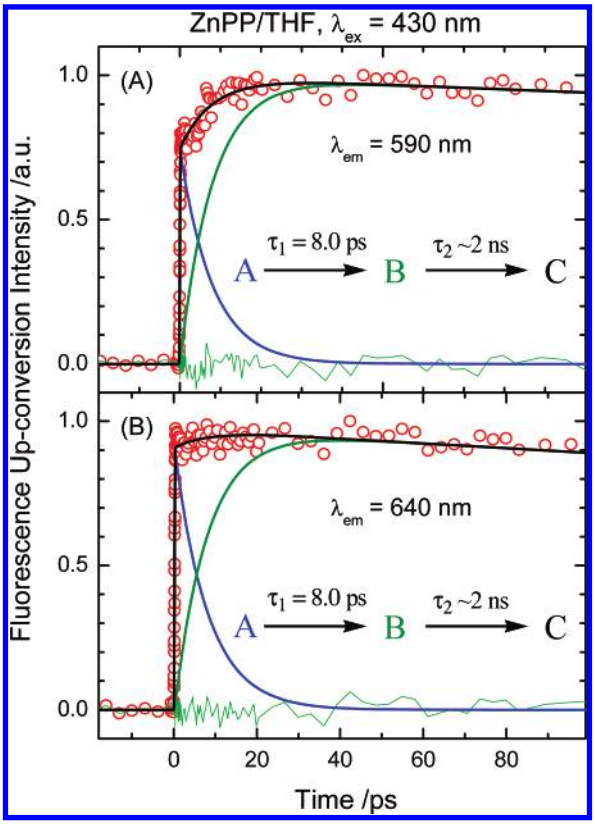

Figure 7. Femtosecond fluorescence transients of ZnPP in THF with λ_{ex} = 430 nm at λ_{em} (nm) = (A) 590 and (B) 640. The red circles denote experimental data; solid black curves represent theoretical fits with a consecutive kinetic model as indicated; blue and olive curves under each transient are deconvoluted components; and green traces represent the residuals of the fit.

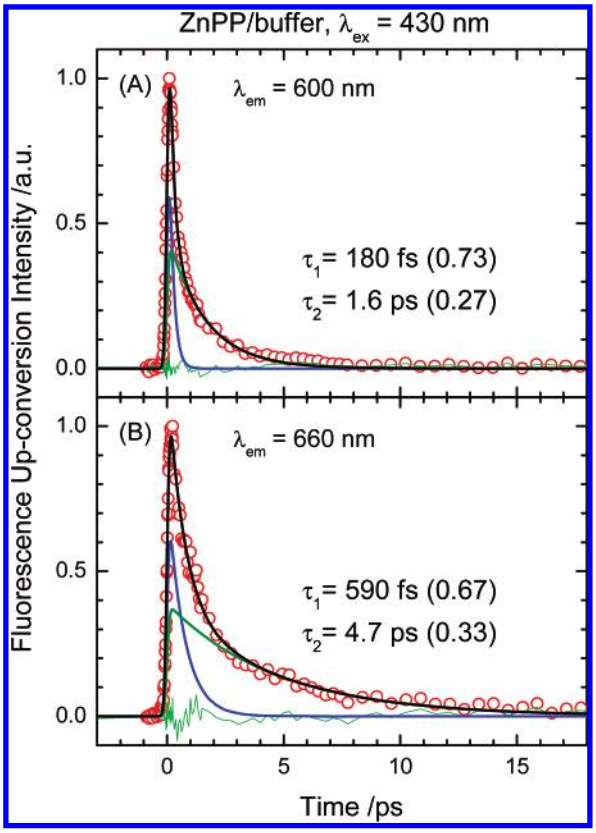

Figure 8. Femtosecond fluorescence transients of ZnPP in buffer solution with λ_{ex} = 430 nm at λ_{em} (nm) = (A) 600 and (B) 660. The red circles denote experimental data; solid black curves represent theoretical fits according to a parallel kinetic model with fitted parameters as indicated; blue and olive curves under each transient are deconvoluted components; and green traces represent the residuals of the fit.

When ZnPP molecules aggregated in buffer solution, we observed that the fluorescence intensity became weak and that the fluorescence relaxation period was limited by the instrument response (<50 ps), which further prevented us from deriving depolarization information for the ZnPP aggregates.

Femtosecond Fluorescence Dynamics of ZnPP Monomers in THF Solution. Figure 7A,B displays femtosecond fluorescence transients of ZnPP in THF solution for the emissions observed at 590 and 640 nm, respectively. The transients feature a prompt rise and a secondary rise to a plateau region on the observed 100 ps scale. Because the excitation populated the S_2 state (λ_{ex} = 430 nm) and the emissions were observed from the S_1 state, the prompt rise in the transients implies that the $S_2 \rightarrow S_1$ internal conversion (IC) might be ultrafast (τ_{IC} < 100 fs). The transient observed in the S_2 state, λ_{ex} = 420 nm and λ_{em} = 470 nm, shows an instrument-limited response (refer to Supporting Information) that is consistent with the transients observed in the S_1 state showing the prompt rise feature. The S_2 emission spectrum of ZnPP in solution was therefore not observed using a commercial spectrofluorimeter in a steady state. τ_{IC} of ZnPP in solution has a value much smaller than those of ZnTPP[6−8] and ZnCAPEBPP[13a] but similar to that of another zinc porphyrin with alkyl substitution at the β-position of the porphyrin ring.[7a] The ultrafast IC relaxation is likely due to the existence of the methyl and vinyl groups at the β-positions of ZnPP so that the CH_3 torsion or the C=C twisting in the S_2 state becomes the driving force for the observed ultrarapid $S_2 \rightarrow S_1$ relaxation.

After the ultrafast $S_2 \rightarrow S_1$ relaxation, we expect that the hot S_1 species (S_1*) were immediately produced. Because the fluorescence transients feature a secondary rise, we employed a consecutive kinetic model, $S_1^* \rightarrow S_1 \rightarrow T_1$, to fit the transients. The two components S_1* and S_1 correspond to hot and cold S_1 species, observed in our fluorescence transients. The component S_1* decays in τ_1 = 8.0 ps, which represents the average duration for vibrational relaxation from the hot S_1 species cooling to form the S_1 species. Consistently, the component S_1 has a rise coefficient of 8.0 ps, but its time constant was fixed at τ_2 = 2 ns as it is insensitive to the fit in the ~100 ps interval, the precise value τ = 2.0 ns we determined from our TCSPC measurements for $S_1 \rightarrow T_1$ ISC. The observed period τ_1 = 8.0 ps for vibrational relaxation in ZnPP/THF solution is consistent with that of ZnCAPEBPP, τ_1 = 8.5 ps,[13a] and that of ZnTPP, τ_1 = ~10 ps,[8] in solutions.

Femtosecond Fluorescence Dynamics of ZnPP Aggregates in Buffer Solution. Because of their slight solubility, to form aggregates in KPi buffer, ZnPP molecules can readily stack together. The effect of aggregation of the ZnPP/buffer system is demonstrated in Figures 1 and 2; here, we provide further evidence for the relaxation dynamics of the ZnPP aggregates upon excitation at λ_{ex} = 430 nm. Figure 8A,B shows the fluorescence transients of ZnPP in KPi buffer with emissions observed at 600 and 660 nm, respectively. Although the transients also feature a prompt rise character, they decay rapidly to the zero-background level on a 10−20 ps scale. A parallel kinetic model with two decay components was employed to fit the transients: the major part of the transient decays in a few hundred femtoseconds (τ_1) and the minor part of the transient decays in several picoseconds (τ_2). At λ_{em} = 600 nm, we obtained the values τ_1 = 180 fs and τ_2 = 1.6 ps; at λ_{em} = 660 nm, τ_1 = 590 fs and τ_2 = 4.7 ps. The nanosecond component

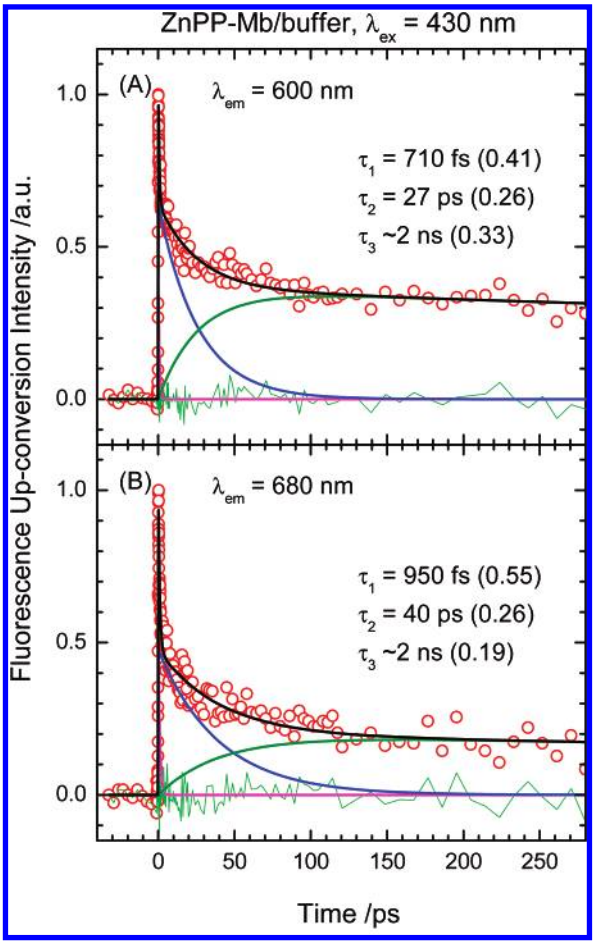

Figure 9. Femtosecond fluorescence transients of the reconstituted ZnPP-Mb in buffer solution with $\lambda_{ex} = 430$ nm at λ_{em} (nm) = (A) 600 and (B) 680. The red circles denote experimental data; solid black curves represent theoretical fits with the fitted parameters as indicated; magenta, blue, and olive curves under each transient are deconvoluted components; and green traces represent the residuals of the fit.

that represents the $S_1 \rightarrow T_1$ ISC of the ZnPP monomer disappeared completely. This behavior indicates that the intermolecular transfer of energy in the ZnPP aggregates was efficient. The resulting two decay components likely reflect aggregates of two types with varied extents of aggregation. The relaxation dynamics depend strongly on wavelength (i.e., the relaxation observed at 600 nm is 3 times as rapid as that observed at 660 nm). This ratio is consistent with the steady-state fluorescence spectrum shown in Figure 2 as the fluorescence intensity at 600 nm is much weaker than that at 660 nm. We infer that the intermolecular transfer of energy in the ZnPP aggregates is more efficient at 600 nm than at 660 nm because (1) spectral overlap between the absorption (Figure 1) and the emission (Figure 2) is greater for the former wavelength and (2) hotter species were observed in the detection window of the former.

Femtosecond Fluorescence Dynamics of ZnPP-Mb in Buffer Solution. Figure 9A,B (the corresponding raw data are shown in Supporting Information) displays the fluorescence transients of reconstituted ZnPP-Mb in KPi buffer for the emission observed at $\lambda_{em} = 600$ and 680 nm, respectively. Both transients exhibit similar dynamical features with a rapid decay followed by a slow decay to an asymptotic offset. The offset component is consistent with the excited state lifetime, $\tau = 2.2$ ns, observed in our TCSPC measurements (Figure 5), but the fast- and slow-decay components were resolved in our femtosecond measurements. Because the fluorescence transients show no apparent rise beyond the initial prompt rise discussed before (Figure 7), the transients were fitted based on a complex kinetic model with three decay components. For the fitted parameters, the three time constants are $\tau_1 = 710$ fs (0.41), $\tau_2 = 27$ ps (0.26), and $\tau_3 = \sim 2$ ns (0.33) at $\lambda_{em} = 600$ nm and $\tau_1 = 950$ fs (0.55), $\tau_2 = 40$ ps (0.26), and $\tau_3 = \sim 2$ ns (0.19) at $\lambda_{em} = 680$ nm; the values in parentheses are relative amplitudes. Because the $S_2 \rightarrow S_1$ IC of the ZnPP monomer occurred extremely rapidly ($\tau_{IC} < 100$ fs), the observed fluorescence transients must arise from the vibrationally hot ZnPP species in the S_1 electronic excited state. We proceed to discuss the observed relaxation dynamics of the hot S_1 ZnPP species.

The observed dynamics of relaxation of ZnPP inside the heme pocket of the apoMb is summarized according to three points. First, because we observed no sub-picosecond relaxation to occur in free solvents, we expect that the observed fast-decay component (τ_1) reflects an efficient energy transfer occurring exclusively from the hot S_1 ZnPP species into the protein. Second, because ZnPP is surrounded by localized water molecules inside the heme pocket of apoMb, we assign the slow-decay component (τ_2) to the water-induced vibrational relaxation of the hot S_1 ZnPP species inside apoMb. The observed relaxation period 27−40 ps is significantly smaller than that of ZnPP in THF, 8 ps, because the water molecules were confined inside the nanocavity of the protein so as to impede the cooling relative to that in free solvents. Third, similar to the ZnPP/THF system, we attribute the nanosecond component τ_3 to the $S_1 \rightarrow T_1$ ISC of the cold ZnPP monomer inside the active site of the protein.

As shown in Figure 9, the relative amplitudes of the fast-decay component and the nanosecond component exhibit a systematic variation, whereas the amplitudes of the slow-decay component remain invariant at both emission wavelengths. When ZnPP monomers were dissolved in THF solution, the contribution of the nanosecond component became dominant because only the excess vibrational energy in the S_1 state was transferred to the surrounding solvents (Figure 7), and the vibrationally relaxed S_1 species fluoresced eventually. When free ZnPP monomers formed aggregates in buffer solution, we observed, however, much more rapid energy relaxation (Figure 8)—the efficient transfer of electronic energy between ZnPP molecules must be involved, so as to extinguish the nanosecond component of the transient. In the ZnPP-Mb/buffer system, we expect the fast-decay component to be due to not only the transfer of vibrational energy in the excited state, which in principle has no effect on the amplitude of the nanosecond component, but also the transfer of the entire electronic energy that diminishes the contribution of the nanosecond component. The relative amplitude of the fast-decay component is larger at $\lambda_{em} = 680$ nm than at $\lambda_{em} = 600$ nm, which indicates that the probe window for the electronic energy transfer is more effective at larger wavelengths. Hotter S_1 species were probed more efficiently at 600 nm than at 680 nm, consistent with the relaxation coefficients τ_1 and τ_2 for which the values observed at 600 nm are less than those observed at 680 nm.

Our direct observation of the dynamics of energy transfer of the ZnPP protein system might be compared with those of the heme protein system for which both experiments[25,27,28] and calculations[23,30] have been conducted. On the basis of computer simulation of the relaxation of vibrational energy, work by Henry et al.[23] indicates that the cooling of the heme in myoglobin and cytchrome *c* is a biphasic process equally weighted with relaxation periods 1−4 and 20−40 ps. Consistently, Mizutani and Kitagawa,[25] who performed time-resolved

resonance-Raman measurements for myoglobin, reported that the biphasic relaxation periods are 3.0 and 25 ps with an amplitude ratio 93:7. In contrast, Straub and co-workers[30] reported their simulation results for the relaxation of vibrational energy of photolyzed heme in myoglobin to follow a single exponential with a time constant 5.9 ps, which agrees with the experimental data of Anfinrud and co-workers.[28] Straub and co-workers[30] proposed three channels for the energy transfer from heme to the surrounding protein and solvent: (1) a through-projectile channel is due to collisions of the photolyzed ligand (CO) with the heme pocket residues; (2) a through-bond channel occurs through the covalent bond between heme and proximal histidine; and (3) a through-space channel involves collisions with solvent molecules.[30]

On the basis of the mechanism for energy transfer provided from the simulations of classical dynamics of myoglobin,[30] we rationalize the relaxation dynamics for our system. Because the excited ZnPP inside apoMb was produced via direct excitation, the through-projectile channel of energy transfer is eliminated. According to simulation results, as the through-space channel dissipates energies via nonbonded transfer of collisional energy from the heme side chains to nearby solvating water molecules, it is less important. Because in the through-space mechanism the surrounding water molecules served as an intermediate heat bath for transfer of thermal energy to myoglobin, this mechanism is consistent with our assignment for the slow-decay component being due to water-induced vibrational relaxation. For the fast-decay component of the transient, we suggest that it is due to an efficient transfer of energy through the dative bond between zinc protoporphyrin IX and the proximal histidine of apomyoglobin. The binding between zinc and histidine in the ZnPP protein is much weaker than the covalent bond between iron and histidine in the heme protein. The through-bond channel of energy transfer thus continuously accumulates energy in the dative bond of the ZnPP-Mb complex, which might eventually lead to the bond dissociation. This mechanism reasonably explains the observed sample degradation when the sample was exposed to laser radiation for a long period (Figures 3 and 4).

Conclusion

Myoglobin is a model system that has been extensively studied to acquire an understanding of the interactions inside the heme pocket of the protein. We prepared a fluorescent protein by removing the heme molecule from myoglobin to form apomyoglobin and reconstituted the ZnPP molecule into the heme pocket of the protein. On the basis of both picosecond time-correlated single-photon counting (TCSPC) and femtosecond fluorescence up-conversion spectroscopy techniques, the present results show explicit experimental evidence for the manner in which the protein matrix influences the relaxation of ZnPP through a comparison of the fluorescence dynamics of ZnPP in THF, KPi buffer (100 mM), and reconstituted within apoMb. The fluorescence transients of the ZnPP-Mb/buffer system exhibit a biphasic decay feature with the signal approaching an asymptotic offset. We conclude that (1) the rapid-decay component reflects an efficient transfer of energy from the hot S_1 ZnPP species to apoMb through the dative bond between zinc porphyrin and proximal histidine of the protein; (2) the slow-decay component pertains to the transfer of vibrational energy from the hot S_1 ZnPP species to apoMb via collisions with the surrounding water molecules; and (3) the offset component is due to the $S_1 \rightarrow T_1$ intersystem crossing of the surviving cold S_1 ZnPP species. The energy transfer through bonds might effectively accumulate thermal energy in the dative bond and eventually leads to dissociation. This mechanism is consistent with our observation showing the degradation of the ZnPP-Mb samples according to absorption and CD spectra upon protracted excitation.

Acknowledgment. We thank Professor S. H. Lin for many insightful discussions. National Science Council of the Republic of China provided financial support under Contract 95-2113-M-009-027. Support from the MOE-ATU program is also acknowledged.

Supporting Information Available: Figures showing raw data of picosecond fluorescence anisotropy for Figure 6 and femtosecond fluorescence transients observed at the S_1 and S_2 states. This material is available free of charge via the Internet at http://pubs.acs.org.

References and Notes

(1) White, I. N. H. *Biochem. J.* **1978**, *174*, 853−861.
(2) Kalyanasundaram, K. *Photochemistry of Polypyridine and Porphyrin Complexes*; Academic Press: London, 1992.
(3) Milgrom, L. R. *The Colours of Life*; Oxford University Press, Inc.: New York, 1997.
(4) Balzani, L.; Credi, A.; Venturi, M. *Molecular Devices and Machines*; Wiley-VCH: Weinheim, Germany, 2003.
(5) Campbell, W. M.; Burrell, A. K.; Officer, D. L.; Jolley, K. W. *Coord. Chem. Rev.* **2004**, *248*, 1363−1379.
(6) Gurzadyan, G. G.; Tran-Thi, T.-H.; Gustavsson, T. *J. Chem. Phys.* **1998**, *108*, 385−388.
(7) (a) Akimoto, S.; Yamazaki, T.; Yamazaki, I.; Osuka, A. *Chem. Phys. Lett.* **1999**, *309*, 177−182. (b) Mataga, N.; Shibata, Y.; Chosrowjan, H.; Yoshida, N.; Osuka, A. *J. Phys. Chem. B* **2000**, *104*, 4001−4004.
(8) Yu, H.; Baskin, J. S.; Zewail, A. H. *J. Phys. Chem. A* **2002**, *106*, 9845−9854.
(9) (a) Yoon, M.-C.; Song, J. K.; Cho, S.; Kim, D. *Bull. Korean Chem. Soc.* **2003**, *24*, 1075−1080. (b) Yoon, M.-C.; Jeong, D. H.; Cho, S.; Kim, D.; Rhee, H.; Joo, T. *J. Chem. Phys.* **2003**, *118*, 164−171.
(10) Kalyanasundaram, K.; Vlachopoulos, N.; Krishnan, V.; Monnier, A.; Grätzel, M. *J. Phys. Chem.* **1987**, *91*, 2342−2347.
(11) Koehorst, R. B. M.; Boschloo, G. K.; Savenije, T. J.; Goossens, A.; Schaafsma, T. J. *J. Phys. Chem. B* **2000**, *104*, 2371−2377.
(12) Viseu, T. M. R.; Hungerford, G.; Ferreira, M. I. C. *J. Phys. Chem. B* **2002**, *106*, 1853−1861.
(13) (a) Luo, L.-Y.; Lo, C.-F.; Lin, C.-Y.; Chang, I.-J.; Diau, E. W.-G. *J. Phys. Chem. B* **2006**, *110*, 410−419. (b) Lo, C.-F.; Luo, L.-Y.; Diau, E. W.-G.; Chang, I.-J.; Lin, C.-Y. *Chem. Commun.* **2006**, 1430−1432.
(14) Labbe, R. F.; Verman, H. J.; Stevenson, D. K. *Clin. Chem.* **1999**, *45*, 2060−2072.
(15) Zhang, Z.; Imae, T. *Nano Lett.* **2001**, *1*, 241−243.
(16) (a) Lin, J.-S.; Chen, Y.-C.; Chen, C.-C.; Diau, E. W.-G.; Liu, T.-F. *J. Chin. Chem. Soc.* **2006**, *53*, 201−208. (b) Lin, J.-S.; Chen, Y.-C.; Chen, C.-C.; Luo, L.-Y.; Diau, E. W.-G.; Liu, T.-F. *J. Chin. Chem. Soc.* **2006**, *53*, 1405−1412.
(17) (a) Maiti, N. C.; Ravikanth, M.; Mazumdar, S.; Periasamy, N. *J. Phys. Chem.* **1995**, *99*, 17192−17197. (b) Maiti, N. C.; Mazumdar, S.; Periasamy, N. *J. Phys. Chem. B* **1998**, *102*, 1528−1538.
(18) Rubtsov, I. V.; Kobuke, Y.; Miyaji, H.; Yoshihara, K. *Chem. Phys. Lett.* **1999**, *308*, 323−328.
(19) (a) Kano, H.; Saito, T.; Kobayashi, T. *J. Phys. Chem. B* **2001**, *105*, 413−419. (b) Kano, H.; Saito, T.; Kobayashi, T. *J. Phys. Chem. A* **2002**, *106*, 3445−3453.
(20) Zimmermann, J.; Siggel, U.; Fuhrhop, J.-H.; Röder, B. *J. Phys. Chem. B* **2003**, *107*, 6019−6021.
(21) Larsen, J.; Andersson, J.; Polívka, T.; Sly, J.; Crossley, M. J.; Sondström, V.; Akesson, E. K. *Chem. Phys. Lett.* **2005**, *403*, 205−210.
(22) (a) Scolaro, L. M.; Castriciano, M.; Romeo, A.; Patane, S.; Cefali, E.; Allegrini, M. *J. Phys. Chem. B* **2002**, *106*, 2453−2459. (b) Castriciano, M. A.; Romeo, A.; Villari, V.; Angelini, N.; Micali, N.; Scolaro, L. M. *J. Phys. Chem. B* **2005**, *109*, 12086−12092.
(23) Henry, E. R.; Eaton, W. A.; Hochstrasser, R. M. *Proc. Natl. Acad. Sci. U.S.A.* **1986**, *83*, 8982−8986.
(24) Miller, R. J. D. *Acc. Chem. Res.* **1994**, *27*, 145−150.
(25) (a) Mizutani, Y.; Kitagawa, T. *Science* **1997**, *278*, 443−446. (b) Kitagawa, T.; Haruta, N.; Mizutani, Y. *Biopolymers* **2002**, *67*, 207−213.
(26) Wang, Y.; Baskin, J. S.; Xia, T.; Zewail, A. H. *Proc. Natl. Acad. Sci. U.S.A.* **2004**, *101*, 18000−18005.
(27) Lakowicz, J. R.; Gratton, E.; Cherek, H.; Maliwal, B. P.; Laczko, G. *J. Biol. Chem.* **1984**, *259*, 10967−10972.

(28) (a) Lim, M.; Jackson, T. A.; Anfinrud, P. A. *J. Phys. Chem.* **1996**, *100*, 12043−12051. (b) Lim, M.; Jackson, T. A.; Anfinrud, P. A. Time-resolved infrared studies of ligand dynamics in heme proteins. In *Ultrafast Infrared and Raman Spectroscopy*; Fayer, M. D., Ed.; Marcel Dekker: New York, 2001; pp 191−226.

(29) (a) Wang, W.; Ye, X.; Demidov, A. A.; Rosca, F.; Sjodin, T.; Cao, W. X.; Sheeran, M.; Champion, P. M. *J. Phys. Chem. B* **2000**, *104*, 10789−10801. (b) Ye, X.; Demidov, A.; Rosca, F.; Wang, W.; Kumar, A.; Ionascu, D.; Zhu, L.; Barrick, D.; Wharton, D.; Champion, P. M. *J. Phys. Chem. A* **2003**, *107*, 8156−8165.

(30) (a) Sagnella, D. E.; Straub, J. E. *J. Phys. Chem. B* **2001**, *105*, 7057−7063. (b) Bu, L.; Straub, J. E. *J. Phys. Chem. B* **2003**, *107*, 10634−10639. (c) Bu, L.; Straub, J. E. *J. Phys. Chem. B* **2003**, *107*, 12339−12345.

(31) (a) Feitelson, J.; Barboy, N. *J. Phys. Chem.* **1986**, *90*, 271−274. (b) Barboy, N.; Feitelson, J. *Biochemistry* **1987**, *26*, 3240−3244.

(32) Albani, J.; Albert, B. *Eur. J. Biochem.* **1987**, *162*, 175−178.

(33) Ilari, A.; Boffi, A.; Chiancone, E. *Arch. Biochem. Biophys.* **1995**, *316*, 378−384.

(34) Aono, S.; Nemoto, S.; Ohtaka, A.; Okura, I. *J. Mol. Catal. A: Chem.* **1995**, *95*, 193−196.

(35) Polm, M. W.; Schaafsma, T. J. *Biophys. J.* **1997**, *72*, 373−382.

(36) (a) Hu, Y.-Z.; Takashima, H.; Tsukiji, S.; Shinkai, S.; Nagamune, T.; Oishi, S.; Hamachi, I. *Chem.—Eur. J.* **2000**, *6*, 1907−1916. (b) Hu, Y.-Z.; Tsukiji, S.; Shinkai, S.; Oishi, S.; Hamachi, I. *J. Am. Chem. Soc.* **2000**, *122*, 241−253.

(37) Teale, F. W. *Biochim. Biophys. Acta* **1959**, *35*, 543.

(38) Hamachi, I.; Tanaka, S.; Shinkai, S. *J. Am. Chem. Soc.* **1993**, *115*, 10458−10459.

(39) EI-Nahass, M. M.; Zeyada, H. M.; Aziz, M. S.; Makhlouf, M. M. *Spectrochim. Acta, Part A* **2005**, *61*, 3026−3031.

(40) Udal'tsov, A. V.; Tosaka, M.; Kaupp, G. *J. Mol. Struct.* **2003**, *660*, 15−23.

(41) Nüesch, F.; Gratzel, M. *Chem. Phys.* **1995**, *193*, 1−17.

(42) Scolaro, L. M.; Romeo, A.; Castriciano, M. A.; Micali, N. *Chem. Commun.* **2005**, 3018−3020.

(43) Euripedes, A.; Ribeiro, J.; Wiliam, C. B. R.; Ljubica, T.; Carlos, H. I. R. *Protein Expression Purif.* **2003**, *28*, 202−208.

(44) Fandrich, M.; Forge, V.; Buder, K.; Kittler, M.; Dobson, C. M.; Diekmann, S. *Proc. Natl. Acad. Sci. U.S.A.* **2003**, *100*, 15463−15468.

(45) Maiti, N. C.; Mazumdar, S.; Periasamy, N. *J. Phys. Chem.* **1995**, *99*, 10708−10715.

(46) Valeur, B. *Molecular Fluorescence*; Wiley-VCH: Weinheim, Germany, 2002; Ch. 6 and references therein.

(47) Lakowicz, J. R.; Gratton, E.; Cherek, H.; Maliwal, B. P.; Laczko, G. *J. Biol. Chem.* **1984**, *259*, 10967−10972.